Modeling Flow Distribution for Internally Manifolded Direct Methanol Fuel Cell Stacks

By *P. Argyropoulos*, *K. Scott*, and *W. M. Taama**

A model is presented for the liquid feed direct methanol fuel cell, which describes the hydraulic behavior of an internally manifolded cell stack. The model is based on the homogeneous two-phase flow theory and mass conservation equation. The model predicts the pressure drop behavior of an individual fuel cell, and is used to calculate flow distribution through fuel cell stack internal manifolds. The flow distribution of the two-phase fluids in the anode and the cathode chambers is predicted as a function of cell operating parameters. An iterative numerical scheme is used to solve the differential equations for longitudinal momentum and continuity.

1 Introduction

Fuel cells produce electricity continuously through the electrochemical oxidation of a fuel. Recent years have seen an upsurge in interest in fuel cells for a range of applications, in particular for transport and smaller scale static power systems. Depending on the load, fuel, cell type and conditions of operation a single cell has a potential of 0.5 V to 1.0 V. To yield a sufficiently high voltage, the cells are stacked, or electrically connected, in series. Stacking of the cells imposes some difficult technological problems. For instance, fuel and oxidant have to flow separately in either side of each cell. This requires some spacing but with electrical contact between each cell maintained. These functions are combined in what is referred to as a bipolar plate.

The interest in fuel cells has, in particular, been generated by the breakthrough in solid polymer electrolyte fuel cells, mainly with hydrogen as the clean source of fuel. The use of hydrogen raises issues of transportation and storage and so an alternative is to reform/oxidize liquid fuel to hydrogen in situ. This alternative raises issues of overall cost and system operation. Consequently, a cell which oxidizes a liquid fuel directly, without reformation, is attractive and several fuels have been proposed and researched, including methanol, methoxymethanes, formic acid, methyl formate, ethanol, etc. A requirement of the fuel is that, on oxidation, a clean combustion to carbon dioxide is achieved. Anticipated temperatures of operation of around 100 °C limit the choice with currently available electrocatalysts to simple species, such as methanol, otherwise organic byproducts are formed in large quantities. Direct methanol fuel cells (DMFC) are emerging as a promising technology due to several advantages, when compared to hydrogen-based systems; no fuel processing unit, resulting in a simpler system with potentially higher volumetric and mass energy densities, possible use of existing fuel supply and distribution system infrastructure. The direct methanol fuel cell (DMFC) uses methanol, as either vapor or liquid, as fuel and operates at relatively low temperatures (< 130 °C). The electrode reactions are:

anode:

$$CH_3OH + H_20 \rightarrow 6e^- + 6H^+ + CO_2$$

cathode:

$$\frac{3}{2}O_2 + 6e^- + 6H^+ \rightarrow 3H_2O$$

which can be combined and give the overall reaction:

$$CH_3OH + \frac{3}{2}O_2 \rightarrow 2H_2O + CO_2$$

Many issues remain to be solved in the design of the system. There are still limitations in components of the cell; electrocatalysts, membranes, bipolar plates and flow beds. Cheaper and more active electrocatalysts, at lower loading (< 1 mg cm^{-2}), are required to reduce cost. Problems exist with membrane materials in terms of methanol transfer, from anode to cathode, which reduces cathode performance. Electrode assembly and cell fabrication materials are still relatively expensive and not optimized.

Development of new materials and effective system design should be based on an in-depth understanding of the system engineering and identification of relevant physical and chemical processes in the cells and their potential interactions. The liquid feed cell produces two-phase flow conditions in the cell; carbon dioxide evolution and dissolution within the liquid phase, and associated vapor-liquid equilibrium between phases. These factors, plus methanol and water transfer (crossover) through the membrane and oxygen consumption at the cathode, represent a complex system. The compact design of the DMFC limits, to a major extent, the ability to observe and monitor the cell internal working environment. An approach to the problem is the combined use of experimental data, and observations, with mathematical modeling. Modeling can provide an insight into the phenomena that cannot be observed experimentally. Many of these phenomena are unique to the DMFC and hence most of the modeling work carried out for the solid polymer hydrogen fuel cells cannot be used for the case of DMFC.

[*] P. Argyropoulos, K. Scott, W. M. Taama, Chemical and Process Engineering Department, University of Newcastle upon Tyne, Merz Court, Newcastle upon Tyne, NE1 7RU, UK.

  0930-7516/00/1111-0985 $ 17.50+.50/0

In previous work we have reported engineering models (thermal, pressure drop, vapor-liquid equilibrium) of the DMFC [1–6]. These individual models were based on the simplifying assumption of equal flow distribution to cells. The purpose of this paper is to model the flow distribution in large direct methanol fuel cell stacks and to predict the effect of system parameters on the flow distribution [6].

2 DMFC Stacks Manifolding

A schematic diagram of a DMFC stack with two cells is shown in Fig. 1. The stack consists of several components:

1. Two stainless steel end plates, to align and compress the stack, two Teflon sheets to isolate the end plates from current collector plates.
2. The bipolar plates for electrical contact between cells and which have flow fields machined on both surfaces for fuel and oxidant flow.
3. Two end plates that have flow fields machined only on one side.
4. Membrane electrode assemblies (MEA). These consist of two electrocatalysts (typically Pt-Ru for the anode and Pt for the cathode), attached to either side of the polymer electrolyte membrane (PEM). Carbon-backing layers serve as support for the uncatalyzed gas diffusion layers and for the catalyst layer. The membrane is electrically insulated at its sides to avoid a cell short-circuit. This insulation material (Teflon^{tm} tape) also serves as a seal for the cell. The membrane electrode assemblies (MEA) are sandwiched between the bipolar plates.

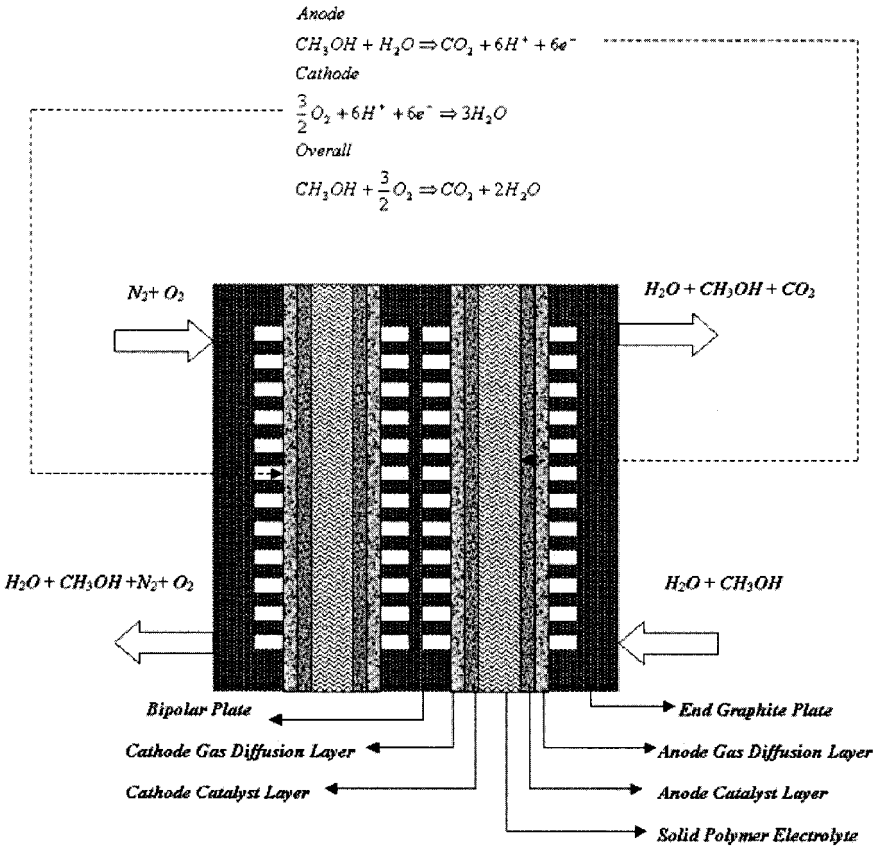

Figure 1. Schematic diagram of the DMFC stack.

The flow bed design for the bipolar plate as shown in Fig. 2 was a result of experimental flow visualization studies of the working environment in the DMFC [7,8]. The design is based on a compact heat exchanger concept. The flow bed is in three sections: a triangular enlarging inlet section, 30 mm long, with a series of 2 mm^2 rectangular spots, a central region of parallel flow channels of 4 mm^2 cross section and a triangular outlet section of a similar design to the inlet section. Methanol solution flows into the cell from a 15 mm diameter inlet port at one corner, at the bottom, of the bipolar (graphite) plate and flows out, with carbon dioxide gas, from a 25 mm port at the opposite corner, at the top, of the cell. The flow bed design for methanol solution and air flow are identical. The supply of air (or oxygen) is to the top of the cell, to assist water removal and minimize cathode flooding. Cathode flooding can impede oxygen penetration to the electrocatalyst layer and lead to a reduction in cell performance.

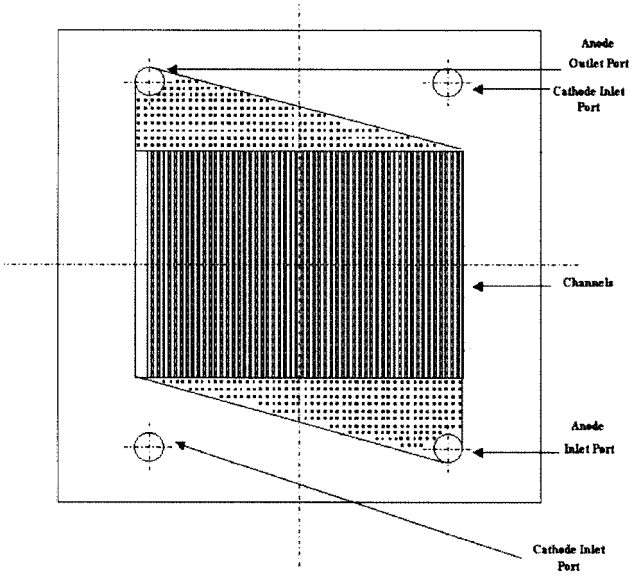

Figure 2. DMFC flow bed design.

The bipolar plates also have a function in the manifolding or distribution of reactants and products and excess reactants. This is the case of internal manifolding (see Fig. 3) where internal channels are located inside the cell stack, as opposed to external manifolding were external channels are used. Both

manifolds have advantages and disadvantages, the balance of which still has to be determined [9]. A manifold can be described as a flow channel (commonly known as header) having a number of discrete openings in the side walls (known as laterals) through which the fluid enters or leaves the header. The simple dividing and combining flow manifolds are the two basic types of manifold. Parallel, reverse and mixed flow arrangements (shown schematically in Fig. 3) are combinations of the basic dividing and combining manifolds interconnected by lateral branches [10].

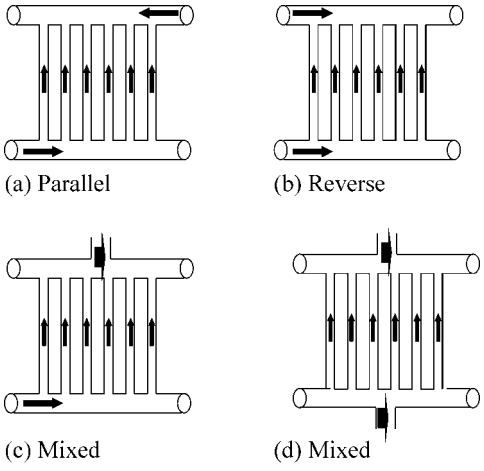

Figure 3. Schematic representation of various flow manifold types.

Examples of the application of manifolds include electrochemical cells, fixed-bed catalytic reactors, hydrocarbon thermal crackers and plate heat exchangers [11]. In the case of electrochemical cells a major disadvantage of internal manifolding is a significant amount of current bypass around the cells. In a fuel cell, such as the DMFC, with a solid polymer electrolyte, the fluids are not ionically conducting and current bypass is not a concern. An aspect of concern in the stacking of fuel cells is how well reactants are distributed to individual cells, especially along a stack with a large number of fuel cells. A nonuniform distribution of reactants will potentially cause differences in the performance of each cell, i.e. cell voltage. The main parameters which affect the flow distribution inside the cell stack are reactant flow rates and hydraulic resistances. These resistances

1. are caused by flow through the manifold channels; the manifold channels can be regarded as pipes with rough surfaces;
2. result from the pressure drop caused by splitting the flow in the inlet manifold channels;
3. results from the pressure drop caused by combining the flow in the outlet manifold channels.

The prototype DMFC stack under development in Newcastle is based on an internally manifolded stack with reverse-type flow arrangement and is presented schematically in Fig. 4. This stack configuration will be used for the model although the model can be used to describe other DMFC stacks by the insertion of a different cell geometry.

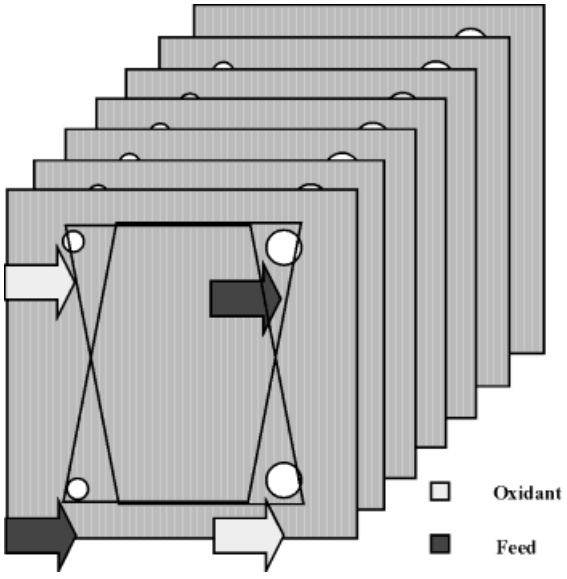

Figure 4. Schematic of an internally manifolded fuel cell stack.

3 Manifold Flow Distribution Characteristics

In general, to achieve a constant and steady operation stack operation, it is necessary to avoid, or minimize, all types of flow maldistribution. If both fluids are not evenly distributed, we can have localized feed or oxidant starvation, which will lower the cell performance. In addition, for the DMFC localized carbon dioxide accumulation can occur causing instabilities in short-term and long-term operation. In the analysis of flow distribution caused by cell manifolding, the analysis used for plate and frame heat exchangers can, with suitable modification, be used with appropriate allowance for phenomena that occur in the DMFC.

In general, there are two important types of possible flow maldistributions; within the channels of the flow fields and manifold-induced. Flow maldistribution in the channels of the flow fields are often caused by the plate bed design. Flow visualization studies (see Fig. 5) showed that the DMFC flow bed design provides a uniform flow distribution and so this type of maldistribution is ignored in our analysis [7,8].

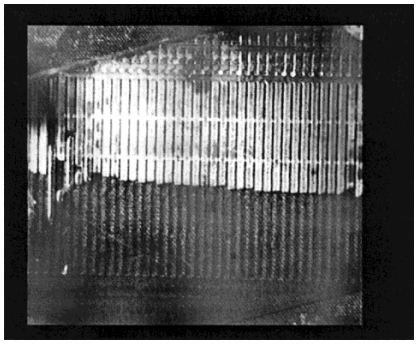

Figure 5. Demonstration of uniform flow distribution in the flow bed design anode-side channels. The photograph shows the liquid flow in the channel as obtained by a video camera.

In a wider context within the channels of the flow fields maldistribution can also be induced from a variety of factors associated with the cell operation, such as:

1. Uneven current distribution as a result of, for example, limited electrical conductivity of current collectors and cell components at high current densities in large cells, and current bypass, will cause variations in carbon dioxide evolution rate in individual channels and thus modify flow behavior. In the DMFC, the absence of liquid electrolyte and the bipolar connection of the cells largely eliminate this effect. However, slight variations in local carbon dioxide generation in individual channels may influence channel flow although this is extremely difficult to determine or predict.
2. Uneven temperature distribution across the flow field, which can affect vapor-liquid equilibrium, boiling initiation, balance between the liquid and gaseous phases and the physical properties of the mixture. The impact of these phenomena is more important for large fuel utilization. In the large-scale system under investigation here large fuel and oxidant excess are used to satisfy thermal and gas management requirements.
3. Flow field design is of paramount importance and, although the present flow bed seems to be satisfactory, in general, the assumption of equal flow distribution should be experimentally verified.

Manifold-induced flow maldistribution occurs at inlet and outlet ports, on a given fluid side in a plate stack, form inlet and outlet manifolds to distribute the fluid in and out of the stack. Different fluid streams, both in composition and throughput, flowing through inlet manifold, plate passages and outlet manifold experience different total flow lengths. Since each fluid stream must experience the same total pressure drop (the difference between inlet and outlet pressures), while flowing through different flow lengths, this can result in flow maldistribution. This effect generally becomes more severe as the number of plates per pass is increased and also in the case of highly viscous liquids being cooled.

Lateral flow is defined here as the flow through a branch of the manifold (i.e., a stacked cell). The lateral flow for a branch of a manifold is primarily determined by the pressure difference between the entrance and the exit of the lateral path and the reaction taking place inside the cell. Three factors affect the pressure in a manifold header and therefore determine flow through lateral paths:

– Pressure drop due to frictional losses
– Pressure recovery
– Pressure drop due to the change in flow bed geometry or system volume

For example, for a dividing flow manifold, frictional losses cause the pressure to drop through the manifold header, while removing fluid through the cell flow fields causes the pressure to increase down the manifold header [11].

There are two important factors that determine the distribution of flow in and from the manifolds:

1. The momentum of the main fluid stream flowing into a manifold tends to carry the fluid toward the closed end, where an excess pressure is produced.
2. Pressure loss due to friction of the fluid against the internal surface of the manifolds.

The former corresponds to change of velocity head. In general, as the fluid flows along the manifold its longitudinal velocity decreases, due to part of the fluid volume being discharged laterally through the openings. Therefore, the fluid flow in the manifold is decreased and, in accordance with Bernoulli's theorem, the fluid pressure increases. Friction, on the other hand, results in loss of pressure along the length. The relative magnitudes of these effects determine whether pressure rises or falls from the inlet to the closed end of the manifold. When the fluid flows into the manifold and undergoes subdivision, i.e., a "blowing manifold", the friction and momentum effects work in opposite directions, the first tending to produce a pressure drop and the second a pressure increase. When the stream is formed in the manifold by the combination of smaller streams and flows from the open end of the main manifold channel, i.e., a "sucking manifold", the friction and momentum effects reinforce each other, creating lower pressures at the open end than at the closed end [12–14].

A fuel cell designer will need to know the pressure drop as well as the extent of nonuniformity in flows through stacks consisting of several cells for a given inlet flow rate. In addition, maintaining friction and momentum effects approximately in balance in a blowing manifold, and estimating the combined effect in a sucking manifold are also design prerequisites.

The flow field in the header of manifold systems can be regarded as one-dimensional, for many practical purposes. However, due to the elliptic nature of the flow in the header, the Bernoulli equation cannot be applied. The difficulty with applying a Bernoulli equation to the branching process lies in the ambiguity which exists in identifying a relevant streamline on which to conserve energy and estimate frictional losses [10,13]. On the other hand, it is necessary to solve simultaneously the longitudinal momentum equation, the continuity equation in the header, and the discharge equation in the cells to obtain the static pressure and the two components of velocity.

Most of the manifold flow distribution models available in the open literature were developed for the case of steam generators [10,18]. Subsequently, they were based on the fact that the mass was conserved in the whole system and simply changed phase (from liquid to gas or vice versa). Unfortunately, this type of analysis is not applicable to the DMFC stack in which mass is consumed/produced from reactions, and water and methanol are transferred through the membrane.

Costamagna has presented a numerical modeling technique for predicting mass flow distribution in fuel cell stacks [19]. This model describes gas-fed fuel cells, using a rectangular duct with multiple openings forming single-pass straight-line channels being discharged to a similar outlet manifold.

Boersma recently presented a model for gas distribution in solid oxide fuel cell stacks but lacked information on flow bed design [20]. The model presented below considers some aspects of that model.

4 Basic Manifold Distribution Model Equations

In a DMFC stack the manifolds are a circular cross section and the channels are rectangular, although other designs, based on different geometries, are under consideration. In the rectangular channels of the graphite bipolar plate the flow is laminar, with very low Reynolds number, while, in the case of circular manifolds, the flow can be either laminar or turbulent depending on the total flow rate in both sides of the cells. The analysis is complicated by the fact that in a DMFC environment there is two-phase flow at the anode side where carbon dioxide bubbles flow with the methanol solution inside the channels, and larger gas pockets are present inside the anode-side outlet manifold. Often, depending on the actual operating temperature, the water and methanol are partly in vapor form (in the case of elevated temperatures and pressures), while at medium temperatures they are both in liquid form.

In any channel the extent of developing flow should be considered. According to Incropera [21], for laminar flow, the required length to reach fully developed flow is given by[1)]

$$\frac{l_{f,req}}{d_{tube}} \approx 0.05\mathrm{Re} \tag{1}$$

where l is the required tube length and d is the tube diameter.

For the case of turbulent flow there is no general satisfactory expression for the entry length but, in general, it is accepted that the length is independent of the Reynolds number and, as a first approximation, can be calculated from an expression of the form:

$$10 \le \frac{l_{l,req}}{d_{tube}} \le 60 \tag{2}$$

We hence assume that fully developed turbulent flow takes place for (l/d) > 10 [21]. The required lengths for fully developed flow to be reached are restricted to a few centimeters close to the inlet and outlet ports. As these lengths are much shorter than the flow bed length, the assumption of fully developed flow is adopted.

The pressure drop, Δp, inside a part of the circular cross section manifold can be calculated from the following equation:

$$\Delta p = \frac{1}{2}\left(\rho u^2 \frac{l(f+k)}{d_h}\right) \tag{3}$$

where d_h is the hydraulic diameter, u the flow velocity, l is the pipe length, ρ is the fluid density, f is the hydraulic resistance coefficient which is strongly dependent upon the Reynolds number, and k is the hydraulic resistance due to flow splitting or combining.

The hydraulic resistance k (available in [22,23]) is fully dependent on the ratio of the flow rate supplied to each cell divided by the remaining flow rate, after the split, for the case of "flow splitting", and similarly for other cases. In the view of many other uncertainties with two-phase flow correlations, the friction factors are adequately represented as [24]:

$$f = \begin{cases} \dfrac{64}{\mathrm{Re}} & for\ \mathrm{Re} < 2000\ (Poiseuille\ equation) \\ \dfrac{0.32}{\mathrm{Re}^{0.25}} & for\ \mathrm{Re} > 2000\ (Blasius\ equation) \end{cases} \tag{4}$$

All quantities that refer to two-phase flow are calculated as weighted averages of the mass fraction of species. Physical properties are calculated for local conditions with the aid of continuous functions.

A critical part in a DMFC stack is the flow bed responsible for reactants/product supply/removal at the electrocatalyst layers. The equation for calculating the pressure drop in the flow beds is:

In this equation, G is the mass velocity (kg m^{-2} sec^{-1}) υ_{fg} is the difference in specific volumes between the gas and liquid phase, υ_{fi} is the liquid specific volume at the inlet temperature, υ_f is the liquid phase specific volume, and υ_g is the gas phase specific volume. All the quantities that refer to two or more component mixtures are calculated as weighted averages based on the component mass fractions. The cell reactions and methanol and water crossover through the membrane are included in the relative mass balances, which are solved locally, to calculate the local value of mass velocity.

$$\Delta p = \int_0^{l_I} \left\{ \begin{array}{c} \left[G^2(y)\left[\dfrac{2(yf(y)+K_I)\upsilon_f(y)}{d_{H,ge}} + \left(\upsilon_f(y) - \upsilon_{fg}(y)\right)\right] + \dfrac{gy}{\upsilon_{fg}(y)}\right] \\ G^2(y)\left[\dfrac{2(yf(y)+K_I)\upsilon_f(y)}{d_{H,ge}} \times \left(\dfrac{1+x_0(y)\upsilon_{fg}(y)}{2\upsilon_f(y)}\right) + \left(\upsilon_f(y) - \upsilon_{fi}(y)\right) + \upsilon_{fg}(y)x_0(y)\right] + \\ \dfrac{gy}{\upsilon_{fg}(y)x_0(y)} \ln\left(\dfrac{1+x_0(y)\upsilon_{fg}(y)}{\upsilon_f(y)}\right) \end{array} \right\} dy \tag{5}$$

1) List of symbols at the end of the paper.

The first part of this equation represents pressure drop for single-phase flow, i.e., with no electrochemical activity or when the maximum solubility (dependent on local temperature, pressure and composition) of carbon dioxide in the aqueous methanol solution is not exceeded. The second part of the above equation has four terms:

1. The first denotes the frictional pressure drop for two-phase flow.
2. The second accounts for the acceleration of the liquid due to a change in the specific volume.
3. The third represents acceleration pressure drop for the two-phase flow.
4. The two-phase gravitational head.

Eq. (5) is used to describe the flow in the inlet and outlet manifolds of the stack.

The velocities at the two ends (x = 0 and x = L) of the manifolds are

1. for the case of a reverse flow dividing manifold:

$$x = 0, \quad \mathrm{u} = \mathrm{u}_{\mathrm{inlet}} = \frac{Q_{inlet}}{\rho \alpha_H} \tag{6}$$

$$x = L, \; u = 0 \tag{7}$$

2. for a combining manifold:

$$\mathrm{x} = 0, \quad \mathrm{u} = \mathrm{u}_{\mathrm{outlet}} = \frac{\mathrm{Q}_{\mathrm{outlet}}}{\rho \alpha_{\mathrm{H}}} \tag{8}$$

$$x = L, \; u = 0 \tag{9}$$

In general, Eq. (5) predicts the following behavior for the anode-side pressure drop of a single cell. The inlet temperature, the methanol concentration or the overall anode-side temperature gradient has a small effect on the overall pressure loss. Volumetric flow rate and current density have a more profound effect on pressure loss. Increasing the flow rate increases the friction losses, while increasing current density reduces overall losses due to the production of more carbon dioxide gas. The model is based on the assumption that the anode liquid is fully saturated with carbon dioxide as in practice the feed is recycled from an external reservoir or from a gas liquid separator.

In its present form the model does not consider the vapor-liquid equilibrium between the water and methanol solution and the gaseous phase. These are the subjects of a separated more detailed and complicated modeling [5]. The scope of this study is to establish a theoretical procedure for manifold designs for a fuel cell stack. Hence, the use of the current mathematical model is focused on stack operating conditions in a range of values where an "optimum" operating point is likely to exist.

The experimental validation of the above model is extremely difficult. The nature of the system, particularly the compact nature of the cell stack and the very low flow bed depths (2 mm), make the insertion of a suitable flow measurement device near the cells' inlet or outlet ports extremely difficult. On the other hand, measurements of a model device are of limited use since the exact stack conditions and, especially, the electrochemical activity cannot be accurately represented. For these reasons the present model is designed as a tool to provide predictions of real stack operation with an aim of optimizing the stack geometry.

5 Solution Methodology

To solve the flow distribution model, initially a uniform flow distribution is applied in all branches. The pressure drop of the manifold is then initially calculated based on this assumption. With the flow rate in the inlet of the individual cells now estimated the cell pressure drop is calculated with the aid of the pressure drop model. That model is able to calculate the composition and the outlet volumetric flow rate. Then, from these results, we can calculate the pressure drop in the exhaust manifold. Theoretically, the pressure drop in each branch should be equal with the adjacent ones, while typically, the pressure drops resulting from the first iteration are not. A correction procedure is then applied as follows. The average value and the standard deviation of all the branches' pressure drops is calculated and also the variance of each branch. The total calculated pressure drop is divided by the anode-side inlet liquid flow rate in order to correlate the pressure drop with the inlet flow rate. This gives a correction factor of pressure drop per unit liquid flow rate. Then the initial inlet guessed flow rates are corrected according to the formula:

$$q_{in,i,cor,p} = q_{in,i} + \left(\sigma \times \frac{Q_{in}}{\sum_i \Delta \mathrm{p}} \right) \tag{12}$$

where, σ, is the i^{th} cells variance. In general, the predicted corrected flow rates are not compatible with continuity for the inlet manifold. Another correction is made to conform with that principle:

$$q_{in,i,cor,c} = q_{in,i,cor,p} + \left(\frac{Q_{in} - \sum_i q_{in,i,cor,p}}{ncs} \right) \tag{13}$$

Then, with the corrected flow rates, another iterative cycle starts. The convergence criterion is determined as:

$$\sigma_k^2 \leq 0.0001 \tag{14}$$

The physical meaning of such a criterion is that all the branch pressure drops will be in a very narrow range around the mean value and will differ by only a few Pa.

6 Predicted Flow Distribution Profiles

There are two areas of interest in the cell stack manifold flow distribution model: first, how well the reactants are distributed to the cells and, secondly, the overall stack pressure drop. The latter determines the auxiliary equipment sizing and sets the limits of feasible, and economically viable,

operating conditions. In our previous model [3,4] we examined the influence of a whole range of operating conditions on the pressure drop characteristics. The conclusions of this were that the critical parameters determining overall stack pressure drop are the methanol solution flow rate and the current density.

6.1 Anode-Side Flow Distribution

Fig. 6 shows typical results of the anode-side flow distribution, i.e., inlet flow rate to every cell, in the stack, as a function of the number of cells in the stack. These results were based on the criterion of an average methanol solution feed flow rate of 1.0 $dm^3\ min^{-1}$ (cell size 272 cm^2, current density 100 mA cm^{-2}, inlet temperature 80 °C, temperature gradient between inlet and outlet port 1 °C). The flow rate is a critical factor not only because it determines the hydraulic behavior of the stack but also because it is a major means by which heat is transferred to the stack body. In addition, the efficiency of carbon dioxide removal is strongly dependent on the liquid-phase flow rate.

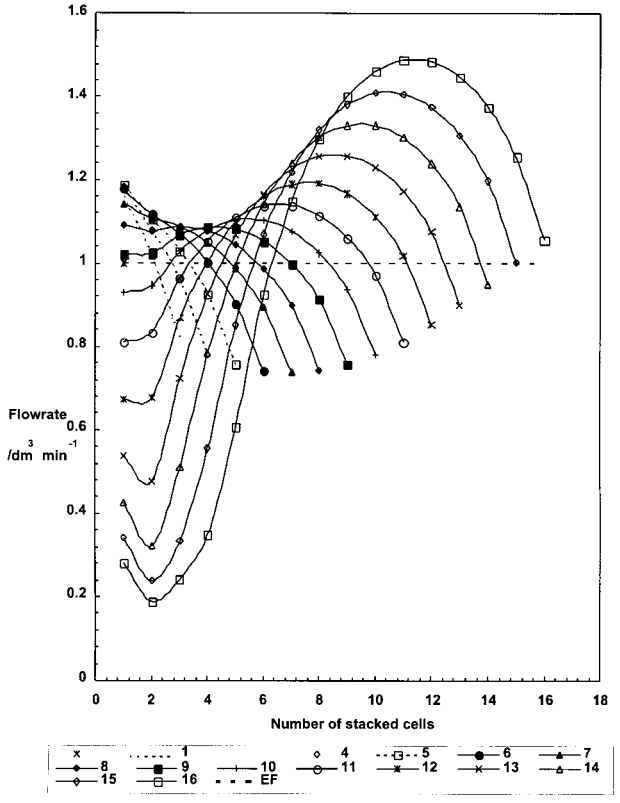

Figure 6. Flow distribution patterns for the anode side of a DMFC stack for increasing number of cells. Volumetric flow rate of 1.0 $dm^3\ min^{-1}$ per cell, 100 mA cm^{-2}, and 80 °C.

As can be seen from Fig. 6, for the specific flow rate per cell, there are severe flow maldistribution problems, especially when the number of cells in the stack exceeds 10. When there are less than 10 cells in the stack, all the cells receive an inlet flow rate in the range of 1.0 ± 0.2 $dm^3\ min^{-1}$. This range is considered as acceptable for electrochemical performance and for stack thermal management. For more than 10 cells the situation deteriorates rapidly. It is indicative that for a 16-cell stack the first cell is fed with only 0.2 $dm^3\ min^{-1}$ of methanol solution. This will result in several potential problems in stack operation particularly under high current load. With a low solution flow rate, and thus a high residence time, high conversions of methanol may cause a significant reduction in methanol concentration and result in a significant fall in individual cell voltage and thus power output. It should be noted that for each 100 mA cm^{-2} of operating current density the stoichiometric flow rate requirement of methanol solution (as 0.5 M) is approximately 0.05 $dm^3\ min^{-1}$. In addition to power loss problems there are also problems of large amounts of carbon dioxide gas generation as discussed below.

It should be noted here that DMFC stack manifolds are a special case. Ideally, the headers should produce a pressure drop much smaller than those of the flow beds so that cell-to-cell flow variations are small. However, the design is constrained by the limited space existing between two adjacent cells and thus the ability to design an adequately large flow distributing manifold. A large manifold will significantly decrease the cell stack volumetric and mass power densities, cause mechanical problems in cell construction and increase the risk of inter-compartment leaks with the derogatory affects on electrode reactions and overpotentials.

In order to understand the significance of this kind of flow maldistribution on the cell performance, a brief discussion of the possible flow patterns in the cells is made. It should be noted that the interactions between carbon dioxide gas evolution, operating conditions and electrochemical performance are complex and are currently the subject of separate research [25,26]. Fig. 7 presents a close-up view of two channels (and 6 channels) of an operating fuel cell (75 °C, 2 bar oxygen cathodic pressure, active area of 102 cm^2) with similar flow bed geometry in use here. It can be seen in Fig. 7a that, for low flow rates (in the range of 0.1–0.2 $dm^3\ min^{-1}$), gas bubbles occupy a large portion of the channel and the flow is essentially that of a gas–liquid dispersion. Thus, the presence of relatively large amounts of carbon dioxide reduces the free area for the flow and reduces, to a great extent, the penetration of reactants to the catalyst layer. This phenomenon is due to the high gas residence time inside the cell, which limits the gas release from the porous gas diffusion layer and results in blocking of the microchannels in that structure. In addition, the greater the carbon dioxide bubble fraction the greater the methanol stripped from the solution, thus decreasing the solution concentration and also causing later problems in methanol recovery and re-use. Fig. 7b shows the two-phase flow in the channels for a flow rate of 1.2 $dm^3\ min^{-1}$ methanol solution. Gas bubbles are fine and efficiently removed. However, parasitic methanol gas stripping may be enhanced due to the high interfacial surface area of fine bubbles. The conclusion drawn from a gas-management point of view is that high flow rates are preferable. High flow rates might also be beneficial for the thermal management of the stack facilitating a more uniform temperature distribution and faster stack

response under varying conditions [1,2]. Although the exact details of the processes occurring in these cases are beyond the scope of the present text, altering the mode of operation can have a major impact on the cell voltage [27]. In practice however, a commercially viable DMFC would be operated with only the feed preheated, (or potentially cooled) before cell entry [6].

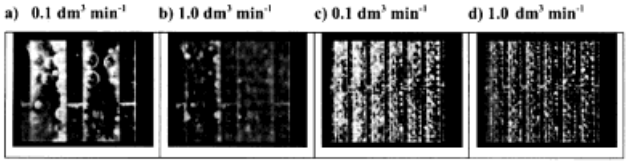

Figure 7. Carbon dioxide evolution patterns for low and high volumetric flow rates. The gas bubbles are in white against the black carbon cloth background.

A major problem with the existing manifold system seems to be the very narrow openings through which methanol solution is fed to the anode-side flow bed. The shallow (only 2.0 mm) flow bed is required for several reasons: relatively thin bipolar plates to reduce Ohmic losses, sufficient mechanical strength due under compression of the stack to achieve proper sealing and minimum system volume (compactness).

Fig. 8 presents anode-side flow distribution patterns for a 10-cell stack as a function of the stack anode-side inlet volumetric flow rate (cell size 272 cm^2, current density 100 mA cm^{-2}, inlet temperature 80 °C, temperature gradient between inlet and outlet port 1 °C). As can be seen, when the flow rate per cell exceeds 1.0 dm^3 min^{-1}, there is a dramatic deterioration in the uniformity of the flow distribution. Nevertheless, for the specific case of the 10-cell stack a cell inlet flow rate in the range of 0.5–1.0 dm^3 min^{-1} gives a reasonable flow distribution. Thus, the conclusion is that a system with high inlet flow rates, containing a large number of stacked cells, will most probably face severe flow maldistribution problems.

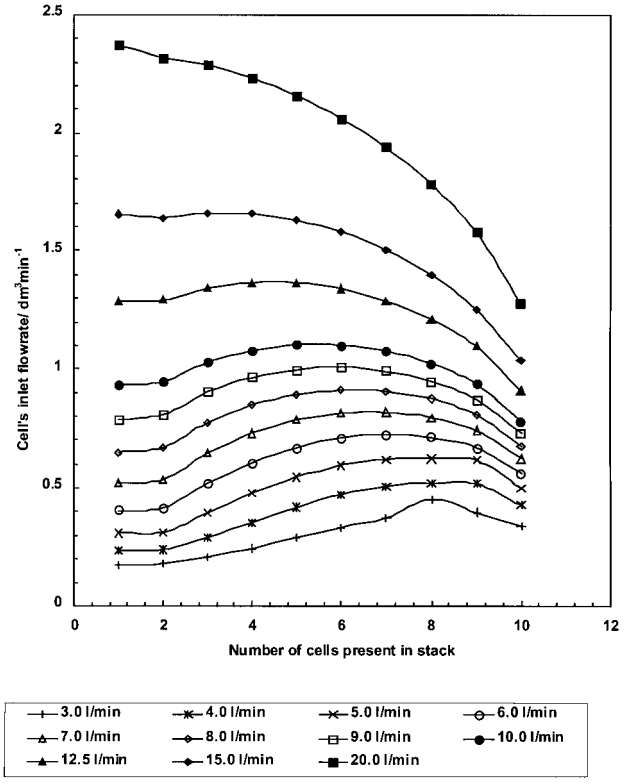

Figure 8. Flow distribution patterns for the anode side of a 10-cell DMFC stack for various volumetric flow rates in dm^3 min^{-1} per cell, 100 mA cm^{-2}, and 80 °C.

6.2 Cathode-Side Flow Distribution

Fig. 9 shows the flow distribution experienced in the cathode side of the DMFC stack when the requirement is for an oxidant supply of 2.0 dm^3 min^{-1}/cell, at 2 bar cathode pressure, 25 °C air inlet temperature and 40 °C cathode-side temperature gradient. There is a serious maldistribution problem experienced in the flow to individual cells. As the number of cells approaches 10, the flow to each individual cell can vary by a factor of approximately 7. The last cells in the stack, farthest away from the inlet and exit, experience the lowest flow, almost 25 % of the design target. This is less critical than for the anode side as it is a main gas flow which is frequently fed in excess above stoichiometric requirements. Hence, even in the case of large variations in individual cell's inlet oxidant flow rate, operating with air excess will secure adequate and sufficient oxidant supply in all cells. Clearly, however, the final cell in the stack will dictate the eventual air flow rate which

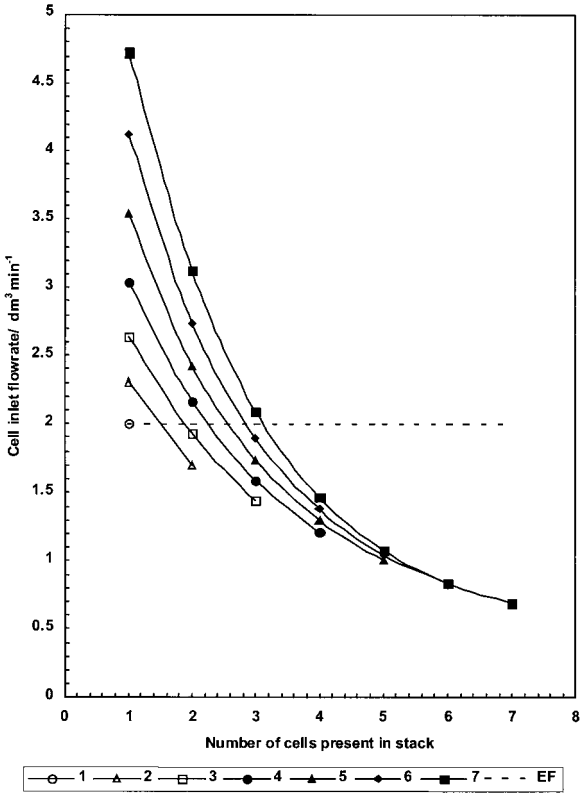

Figure 9. Flow distribution patterns for increasing number of cells, for the cathode side of a DMFC stack for a volumetric flow rate of 2.0 dm^3 min^{-1} per cell, 100 mA cm^{-2}, and 2 bar cathodic pressure.

must be above stoichiometric requirements and also prevent problems of cathode flooding. However, the situation will lead to an excess supply of air to other cells and thus to the stack overall with penalties of higher cost of ancillary stack equipment (pumps, pipes, etc.), and high parasitic power requirements. In addition, the additional air requirements will intensify the problem of recovery of methanol, transferred by electroosmosis from the anode, from the air stream.

7 Overall Stack Pressure Drop Prediction

The total anode-side stack pressure drop is a quantity that is of interest and affects parasitic power requirements to auxiliary pumps. The cathode-side pressure drop is, in comparison, relatively small [3,4] and is generally of less concern, except from the point of view that an overspecification of air, to ensure minimal excess stoichiometric requirements will, as discussed above, result in an increased pumping demand to the cell stack. It is expected that the fluid flowing through the relatively narrow, free spaces in the flow beds will loose a significant amount of energy in the form of friction losses. As the single-cell pressure drop model indicated, there are two critical factors: anode-side inlet flow rate and current density.

Fig. 10 presents the total anode-side pressure drop for cell stacks with 1 to 10 cells and for four different cell inlet volumetric flow rates (cell size 272 cm^2, current density 100 mA cm^{-2}, inlet temperature 80 °C, temperature gradient between inlet and outlet port 1 °C). These flow rates cover a design range from low (0.25 dm^3 min^{-1}/cell) to relatively high (2.0 dm^3 min^{-1}/cell). The predicted pattern is an almost linear increase of the total pressure drop with the number of stacked cells. As the flow rate increases, there is a departure from linearity probably due to the severe flow maldistributions. The overall pressure drop for a 10-cell stack is relatively high of the order of 0.6–1.0 bar.

Fig. 11 shows the overall pressure drop for a 10-cell stack as a function of the stack inlet volumetric flow rate (cell size 272 cm^2, current density 100 mA cm^{-2}, inlet temperature 80 °C, temperature gradient between inlet and outlet port 1 °C). This figure shows that the overall system pressure drop performance, as expected, increases with increasing flow rate. On using a low flow rate (3.0 dm^3 min^{-1}), moderately close to the stoichiometric requirements needed at high current densities (400 mA cm^{-2}), the pressure drop is ≈ 0.45 bar. This condition is approximately equivalent to a 67 % conversion of methanol (assuming a 0.5 M feed concentration). This compares with the case of large fuel excess (20.0 dm^3 min^{-1}) when a greater, overall pressure drop of 1.0 bar occurs. The effect of flow maldistribution is again apparent in this data, as there is an increase in the slope of the line close to an inlet flow rate of 10.0 dm^3 min^{-1}.

Current density was found to be beneficial in reducing the single-cell anode-side pressure drop. That effect is noticeable at low flow rates (< 2.0 dm^3 min^{-1}) and becomes less significant

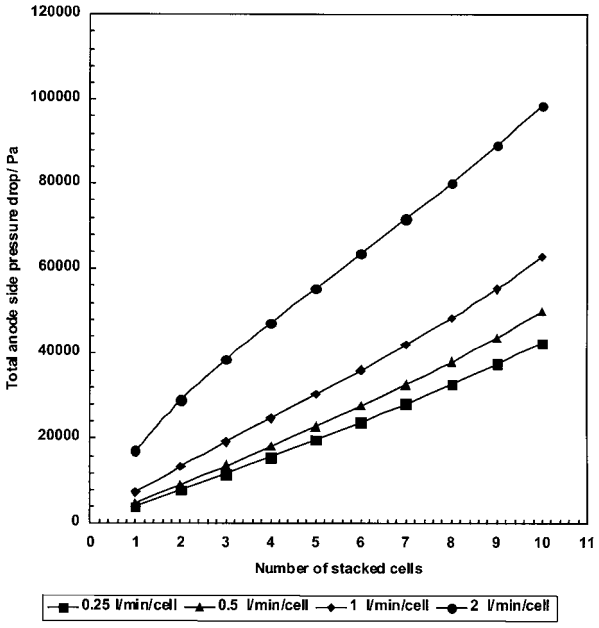

Figure 10. Overall anode-side pressure drop for increasing number of cells present in stack, and various volumetric flow rates in dm^3 min^{-1} per cell, 100 mA cm^{-2}, and 80 °C.

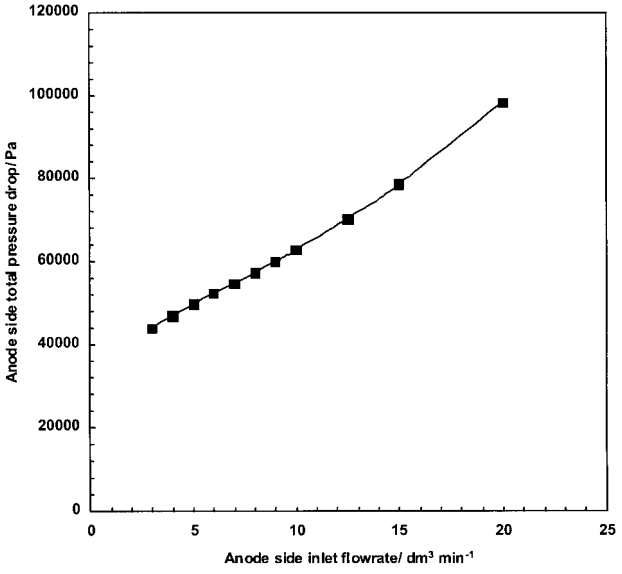

Figure 11. Effect of increasing anode-side inlet flow rate on the overall anode-side pressure drop for a 10-cell stack and a current density of 100 mA cm^{-2}, at 80 °C.

at higher flow rates. The reason behind this behavior is in the ratio of gas to liquid in the flow bed. For small liquid flow rates the gas is present as gas bubbles or slugs that create a "gas lift" effect, reducing the pressure drop. When the liquid-phase flow rate is large, the gas is present as very fine bubbles, with minimum lifting ability, and at the same time the friction and gravitational acceleration related pressure losses have increased.

Fig. 12 shows the effect of current density on overall pressure drop for an increasing number of cells, for cell anode-side inlet flow rate of 1.0 dm^3 min^{-1}/cell, cell size 272 cm^2, inlet

temperature 80 °C and temperature gradient between inlet and outlet port 1 °C. These results show that current density does not affect the overall anode pressure drop significantly. Also, the higher the current density the lower the pressure drop. This is in agreement with the previously mentioned conclusions from the single-cell pressure drop model [3,4]. In addition, increasing the current density increases the amount of carbon dioxide produced and hence the volumetric flow rate at the outlet manifold, resulting in an increase in pressure losses in that part of the stack. The positive effect of the gas lift inside the cell is partly counteracted by the friction losses in the combining manifold and this is the reason for the very small differences in the pressure variations.

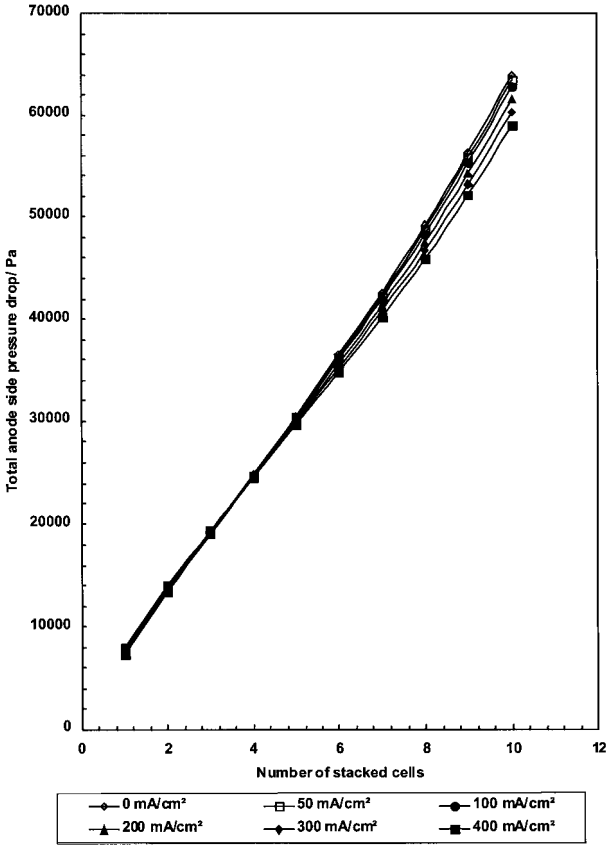

Figure 12. Effect of increasing current density on the overall anode-side pressure drop for a 10-cell stack and volumetric flow rate of 1.0 $dm^3\ min^{-1}$ per cell, at 80 °C.

8 Conclusions

A model has been developed that predicts the flow distribution and the overall stack pressure drop characteristics. There are two areas of interest: first, how well the reactants are distributed to the cells, and secondly, what is the overall stack pressure drop which determines the auxiliary equipment sizing and parasitic power consumption and thus sets the limits of the feasible and economically viable range of operating conditions.

It has been shown that flow maldistribution problems will occur when the number of cells in the stack exceeds 10. The use of lower flow rates tends to give a more uniform flow distribution pattern.

The overall stack anode-side pressure drop increases with increasing liquid inlet flow rate and number of stacked cells and very slightly decreases with increasing current density. The existing manifold design is far from optimized from the point of minimizing parasitic power and thus maximizing power output, but essentially it is dictated by requirements of the electrochemical process, and minimizing the system volume in practical applications.

Acknowledgements

The authors would like to acknowledge the following:
1. The European Commission for supporting Dr P. Argyropoulos under a B20 TMR Marie Curie research training grant.
2. EPSRC for supporting Dr. W. M. Taama.

Received: February 1, 2000 [CET 1201]

Symbols used

A	[m^2]	area
C	[mol dm^{-3}]	concentration
d_H	[m]	hydraulic diameter
f	[–]	friction factor
F	[A sec mol^{-1}]	Faraday constant
G	[kg m^{-2} sec^{-1}]	mass velocity
g	[m sec^{-2}]	standard gravitational acceleration
j	[mA cm^{-2}]	current density
k	[–]	hydraulic resistance
L	[m]	length
M	[10^{-3} kg mol^{-1}]	molecular weight
W		
$\dot{m}$	[kg sec^{-1}]	mass flow rate
n	[–]	number of electrons transferred through the cell
N	[–]	number of channels
P	[Pa]	pressure
p	[Pa]	vapor pressure
Q	[m^3 sec^{-1}]	volumetric flow rate
Re	[–]	Reynolds number
T	[K]	temperature
x_o	[–]	mass fraction of the dispersed phase

Greek symbols

μ	[kg m^{-1} sec^{-1}]	viscosity
ρ	[kg sec^{-1}]	density
υ	[kg m^{-3}]	specific volume
χ	[–]	electrosmotic drag coefficient

Subscripts

d	depth
F	liquid
fb	flow bed
fg	(liquid-gas)
g	gas
gf	(gas-liquid)
mea	membrane electrode assembly
w	width
L	length

References

[1] Argyropoulos, P.; Scott, K.; Taama, W. M., One-Dimensional Thermal Model for DMFC Stacks. Part II. Model-Based Parametric Analysis and Predicted Temperature Profiles, *J. Power Sources 79 (1999) No. 2, pp. 184–198.*

[2] Argyropoulos, P.; Scott, K; Taama, W. M., One-Dimensional Thermal Model for DMFC Stacks. Part I. Model Development, *J. Power Sources 79 (1999) No. 2, pp. 169–183.*

[3] Argyropoulos, P.; Scott, K.; Taama, W. M., Pressure Drop Modelling for Liquid Feed Direct Methanol Fuel Cells (DMFCs). Part II. Model-Based Parametric Analysis, *Chem. Eng. J. 73 (1999) No. 3, pp. 229–245.*

[4] Argyropoulos, P.; Scott, K.; Taama, W. M., Pressure Drop Modelling for Liquid Feed Direct Methanol Fuel Cells (DMFCs). Part I. Model Development, *Chem. Eng. J. 73 (1999) No. 3, pp. 217–227.*

[5] Argyropoulos, P.; Scott, K.; Taama, W. M., Modelling Pressure Distribution and Anode/Cathode Streams Chemical Composition in Direct Methanol Liquid Feed Fuel Cells, *Chem. Eng. J. (1999), accepted.*

[6] Scott, K.; Argyropoulos, P.; Taama, W. M., Modelling Transport Phenomena and Performance of Direct Methanol Fuel Cell Stacks, *IChemE Transactions (2000), accepted.*

[7] Argyropoulos, P.; Scott, K.; Taama, W. M., Gas Evolution and Power Performance in Direct Methanol Fuel Cells, *J. Appl. Electrochem. 29 (1999) pp. 661–669.*

[8] Argyropoulos, P.; Scott, K.; Taama, W. M., Carbon Dioxide Evolution Patterns in Operating DMFC Cells, *Electrochimica Acta 44 (1999) pp. 3575–3584.*

[9] Appleby, A. J., *Characteristics of Fuel Cells Systems, in: Fuel Cell Systems (L. J. M. Blomen, M. N., Ed.) Plenum Press, London 1993, pp. 157–173.*

[10] Datta, A. B.; Majumdar, A. K., A Calculation Procedure for Two-Phase Flow Distribution in Manifolds With and Without Heat Transfer, *Int. J. Heat & Mass Transfer 26 (1983) No. 9, pp. 1321–1328.*

[11] Riggs, J. B., Development of an Algebraic Design Equation for Dividing, Combining, Parallel, and Reverse Flow Manifolds, *Ind. & Eng. Chemistry Research 26 (1987) pp. 129–133.*

[12] Acrivos, A.; Babcock, B. D.; Pigford, R. L., Flow Distribution in Manifolds, *Chem. Eng. Sci. 10 (1959) pp. 112–124.*

[13] Bajura, R. A.; Jones, E. H., Flow Distribution Manifolds, *J. Fluids Eng. (Dec., 1976) pp. 654–666.*

[14] Keller, J. D., The Manifold Problem, *J. Appl. Mechanics (1949) pp. 77–85.*

[15] Majumdar, A. K., Mathematical Modelling of Flows in Dividing and Combining Flow Manifolds, *Appl. Mathematical Modelling 4 (1980) pp. 424–432.*

[16] Datta, A. B.; Majumdar, A. K., Flow Distribution in Parallel and Reverse Flow Manifolds, *Int. J. Heat & Fluid Flow 2 (1980) No. 4, pp. 253–262.*

[17] Bajura, R. A., A Model for Flow Distribution in Manifolds, *J. Eng. Power (Jan., 1971) pp. 7–12.*

[18] Horlock, J. H., An Investigation of the Flow in Manifolds with Open and Closed Ends, *J. Royal Aeronautical Society 60 (1956) pp. 749–753.*

[19] Costamagna, P.; Arato, E.; Achenbach, E.; Reus, U., Fluid Dynamic Study of Fuel Cell Devices: Simulation and Experimental Validation, *J. Power Sources 52 (1994) pp. 243–249.*

[20] Boersma, R. J.; Sammes, N. M., Distribution of Gas Flow in Internally Manifolded Solid Oxide Fuel Cell Stacks, *J. Power Sources 66 (1997) pp. 41–45.*

[21] Incropera, F. P.; DeWitt, D. P., *Introduction to Heat Transfer, 3rd ed., John WILEY & Sons, Inc., New York (USA) 1996.*

]22] Beitz, W.; Kuttner, K.-H., *Dubbel: Handbook of Mechanical Engineering (M. Shields, Ed.) Springer-Verlag, Heidelberg 1994.*

[23] *VDI Wärme-Atlas: Berechnungsblätter für den Wärmeübergang, Verein Deutscher Ingenieure, Düsseldorf 1991.*

[24] Walas, S. M., *Chemical Process Equipment: Selection and Design, Butterworth-Heinemann Series in Chem. Eng. (H. Brenner, Ed.) Butterworth-Heinemann, Boston (USA) 1990.*

[25] Scott, K.; Taama, W. M.; Argyropoulos, P., Engineering Aspects of the Direct Methanol Fuel Cell System, *J. Power Sources 79 (1999) No. 1, pp. 43–59.*

[26] Argyropoulos, P.; Scott, K.; Taama, W. M., *Engineering and Modeling Aspects on Large-Scale Liquid Feed DMFC Stacks, in: 5th Europ. Symp. on Electrochem. Eng. (1999), Exeter, UK: IChemE.*

[27] Argyropoulos, P.; Scott, Yiannopoulos, P.; Taama, W. M., Direct Methanol Fuel Cell Flow Bed Design & Materials. Part II: Electrochemical and Power Performance, *Submitted J. Appl. Electrochemistry (1999).*

